

Article

Phosphate Recovery Mechanism from Low P-Containing Wastewaters via CaP Crystallization Using Apatite as Seed: Seed Adsorption, Surface-Induced Crystallization, or Ion Clusters Aggregation?

Xiaobao Nie ^{1,2,*}, Yinan Li ¹, Junli Wan ^{1,2}, Shuai Ouyang ¹, Zhengbo Wang ¹, Guoqi Wang ¹ and Heng Jiang ³

¹ School of Hydraulic & Environmental Engineering, Changsha University of Science and Technology, No. 960, Section 2, Wanjiashi South Road, Tianxin District, Changsha 410114, China; liyinancsust@163.com (Y.L.); wanjunli@csust.edu.cn (J.W.); ouyangshuaicsust@163.com (S.O.); wangzhengbocsust@163.com (Z.W.); wangguoqicsust@163.com (G.W.)

² Key Laboratory of Dongting Lake Aquatic Eco-Environmental Control and Restoration of Hunan Province, Changsha 410114, China

³ Hunan Water Resources and Hydropower Survey, Design, Planning and Research Co., Ltd., Changsha 410007, China; jiangheng01@126.com

* Correspondence: niexiaobao@csust.edu.cn

Abstract: Low P-containing wastewaters (LPWs) exhibit huge P recovery potential, considering their larger volume. P recovery via CaP crystallization using apatite as seed is documented as being potentially well suited for LPWs. However, its responsible mechanisms remain a subject for debate. Taking hydroxyapatite (HAP) as the seed of LPWs, this paper conducted HAP adsorption/dissolution experiments, titration experiments, and P recovery experiments to distinguish the primary responsible mechanism. Results showed that it was HAP dissolution, not P adsorption, that occurred when the initial P concentration was no higher than 5 mg/L, ruling out adsorption mechanism of P recovery from LPWs using HAP as the seed. Significant OH⁻ consumption and rapid P recovery occurred simultaneously within the first 60 s in titration experiments, suggesting CaP crystallization should be responsible for P recovery. Moreover, the continuous increase in P recovery efficiency with seed dosages observed in P recovery experiments seemed to follow well the mechanism of pre-nucleation ion clusters (PNCs) aggregation. During PNCs aggregation, P aggregates with Ca²⁺ quickly, generating CaP PNCs; then, CaP PNCs aggregate with seed particles, followed by CaP PNCs fusion, and ultimately transform into fines attached to the seed surface. PNCs' aggregation mechanism was further supported by a comparison of seed SEM images before and after P recovery, since denser and smaller rod-shaped fines were observed on the seed surface after P recovery. This study suggests that PNCs' aggregation is the dominant mechanism responsible for the recovery of P from LPWs via CaP crystallization using HAP as the seed.

Keywords: low P-containing wastewater; P recovery; CaP crystallization; ion clusters; aggregation



Citation: Nie, X.; Li, Y.; Wan, J.; Ouyang, S.; Wang, Z.; Wang, G.; Jiang, H. Phosphate Recovery Mechanism from Low P-Containing Wastewaters via CaP Crystallization Using Apatite as Seed: Seed Adsorption, Surface-Induced Crystallization, or Ion Clusters Aggregation? *Separations* **2024**, *11*, 138. <https://doi.org/10.3390/separations11050138>

Academic Editor: Dimosthenis Giokas

Received: 24 March 2024

Revised: 24 April 2024

Accepted: 28 April 2024

Published: 30 April 2024



Copyright: © 2024 by the authors. Licensee MDPI, Basel, Switzerland. This article is an open access article distributed under the terms and conditions of the Creative Commons Attribution (CC BY) license (<https://creativecommons.org/licenses/by/4.0/>).

1. Introduction

Phosphorus (P) is the key element responsible for eutrophication of water bodies [1], resulting in a series of notable problems for different purposes of water use. However, P is also a limited and nonrenewable mineral resource, of utmost importance for the development of human society [2]. According to the last summary of the U.S. Geological Survey, the worldwide phosphate rock reservoirs amount to 71×10^3 Tg, while the excavated phosphate rock amount equaled 223 Tg in 2020 [3]. As a result, many countries have welcomed the suggestion of P recovery from wastewater and are trying to put it into practice [4].

Low P-containing wastewaters (LPWs) refer to those which have a P concentration no higher than 30 mg/L [5]. Municipal wastewater and effluents from industrial fields, such

as paper making [6], printing and dyeing [7], and pharmaceuticals [8], are typical LPWs. LPWs exhibit huge P recovery potential due to their larger volume. However, their low cost-efficiency for P recovery is also well known, because of the low P concentration [9–12]. For example, Xie et al. [10] reported poor P recovery via CaP crystallization when P concentration was below 100 mg/L. P recovery from LPWs via adsorption processes still faces challenges due to the low adsorption affinity and interference of co-existence anions [9,13]. Electrodialysis is a promising technology in regard to recovering P from LPWs [14–16]. However, its application is little discussed [12].

Apatite, including hydroxyapatite (HAP) and its precursor phases, are demonstrated to favor P recovery from wastewater when used as seed particles [17–19]. Two mechanisms, calcium phosphate (CaP) crystallization and P adsorption, are well documented to be associated with this recovery process. On the one hand, apatite acts like a catalyst, lowering the activation energy barrier for CaP crystallization [20]. Furthermore, compared to other medias, such as magnetite minerals [21], steel slags [22], and calcite limestone [23], apatite has been proved to possess the most excellent catalysis performance for LPWs [19,20,24]. For example, using cow bone as seed particles, of which the main content is HAP [24], a P recovery efficiency of 60–90% from LPWs was reported. For secondary effluent from sewage treatment plant, 90% of P recovery was achieved taking HAP as seed [25]. On the other hand, apatite has proved to be a suitable P adsorbent for LPWs due to the great chemical affinity between P and the media [25,26]. Boeykens et al. [26] suggested the adsorption was predominantly produced by ionic exchange processes. Park et al. [27] reported an exchange mechanism where phosphate hydrolysis products were adsorbed on the surface of crawfish char, of which the main content was also HAP. Another mechanism, the attraction between the O-H groups and phosphate ions, was documented to play a key role during P adsorption [26].

However, P adsorption and crystallization from LPWs using apatite are complex mechanisms, and distinguishing between the two is not easy, considering that similar chemical bonds could be involved and both are surface reactions [17]. Søvik et al. [28] declared that adsorption occurred almost instantaneously and was rapidly followed by the precipitation of HAP, while other researchers suggested an adsorption mechanism at low P content and precipitation mechanism at high P content [29,30].

Moreover, even with crystallization being the key mechanism, two distinct crystallization pathways, induced surface precipitation and ions cluster aggregation, may be involved in this process. The former is known as heterogeneous precipitation, wherein nucleation takes place on the seed particles surface [31], while the latter is accomplished through the aggregation between pre-nucleation ion clusters (PNCs) and seed particles [32]. Recently, PNCs have been well documented, even in undersaturated solutions based on in situ measurements, such as in situ small-angle X-ray scattering (SAXS), in situ X-ray absorption spectroscopy (XAS), and in situ high-energy X-ray diffraction (HEXRD) [33–35]. Keeping this in mind, the PNCs' aggregation mechanism seems to be more appropriate because of the low supersaturation of LPWs with respect to CaP.

The overall objective of this study was therefore to illuminate the P recovery mechanism from LPWs via CaP crystallization. The specific aims of this study were as follows: (1) determine whether P adsorption by HAP occurs or not in LPWs; (2) evaluate the role of Ca^{2+} in P recovery from LPWs via CaP crystallization; (3) verify the potential impact of pH, HAP dosage, and crystallization time on P recovery efficiency; (4) examine the exact P recovery mechanism from LPWs via CaP crystallization. HAP, the most thermodynamically stable phase of apatite, was selected as the model seed material for this research. The outcome of this research was anticipated to have important impacts on the development of a preferred alternative for P recovery from LPWs.

2. Materials and Methods

2.1. Materials

Analytical grade reagents, purchased from Sinopharm Chemical Reagent Co., (Shanghai, China) without further purification, have been used in all experiments. The test water used in experiments was deionized water, which had a conductivity of 0.7 $\mu\text{S}/\text{cm}$. LPWs were simulated by dissolving $\text{Na}_2\text{HPO}_4 \cdot 7\text{H}_2\text{O}$ in deionized water. CaCl_2 was used to provide Ca^{2+} source. pH adjustment was achieved with 0.5 M HCl and NaOH solutions, and ionic strength was adjusted by the addition of NaCl.

Seed material, HAP, was purchased from Jinheng Chemical Reagent Co., (Xi'an, China), of which the phases were composed mainly of HAP and its precursor phases (ACP and OCP), with Ca/P molar ratio of 1.83.

2.2. P Adsorption Experiments

P adsorption experiments were carried out by batch method. Determined amounts of HAP (0.1–5 g/L) were suspended in 0.1 M NaCl solution as background electrolyte in 250 mL glass conical flasks pre-cleaned with 1% HNO_3 and cleaned several times with deionized water. The initial P concentration range of the suspension was set at 0–40 mg/L. This range of concentration was selected in order to assess either P adsorption or HAP dissolution predominated in LPWs without Ca^{2+} addition. After that, the pH of the suspension was adjusted to 9.0. The conical flasks were then shaken in an orbital incubator at 200 rpm for 40 h at 298 K. During adsorption, 5 mL aliquots were collected at predetermined time intervals using 0.45 μm membrane syringe filters and measured for P concentration.

In order to elucidate the adsorption process of P on HAP surface, pseudo-first-order, pseudo-second-order, and intra-particle diffusion kinetic models were selected to fit the kinetic data. Their linear forms are given as follows, according to Cheng et al. [13]:

$$\ln(q_e - q_t) = \ln q_e - k_1 t \quad (1)$$

$$\frac{t}{q_t} = \frac{1}{k_2 q_e^2} + \frac{t}{q_2} \quad (2)$$

$$q_t = k_p t^{1/2} + C \quad (3)$$

where q_e and q_t are the P adsorption capacities for HAP (mg/g) at equilibrium and at time t , respectively; k_1 is the rate constant of pseudo-first-order kinetic model (1/min); k_2 is the rate constant of pseudo-second-order kinetic model (g/(mg·min)); k_p is the intra-particle diffusion rate constant (mg/(g·min^{-1/2})); and C is the intercept (mg·g).

Thermodynamic experiments were conducted at 283, 293, and 303 K, respectively.

2.3. Titration Experiments

To monitor CaP crystallization in LPWs, a computer-controlled titration system, 907 Titrando (Metrohm, Switzerland) was used in constant pH titration mode. A 20 mL aliquot of a CaCl_2 solution was added to 180 mL LPWs with 0.4 g HAP, resulting in Ca^{2+} concentration of 3, 30, and 60 mg/L, respectively, P concentration of 1 mg/L, and HAP dosage of 2 g/L. The mixture was rapidly titrated to pH 9.0 with 0.5 M NaOH. Once reaching the pH of the set point (designated as 0 s), CaP crystallization was immediately triggered by a magnetic stirrer at 500 rpm. The extent of crystallization was monitored by following the consumption of NaOH added to maintain constant pH. For each experiment, the reaction was monitored for a total of 1 h at 2 s intervals. A temperature of 298 K was maintained by an external water bath. pH was measured with a pH electrode (Metrohm No. 6.0262.100), calibrated prior to each experiment.

To evaluate the P recovery efficiencies related to base consumption, four 5 mL aliquots were withdrawn from each experiment using 0.45 μm membrane syringe filters and measured P concentration, at characteristic periods before, after, and around the rapid increase in base consumption, corresponding to 0, 60, 1800, and 3600 s.

For further insights into the P recovery mechanism, another titration experiment was conducted in non-constant pH titration mode at seed dosage of 2 g/L and initial pH of 9.0, with initial Ca^{2+} and P concentration of 30 mg/L and 1 mg/L, respectively. CaP crystallization was immediately triggered, as mentioned earlier. pH and electrical conductivity were monitored for a total of 1200 s in 2 s intervals with pH electrode and electrical conductivity electrode (Metrohm No. 6.0916.040), respectively.

2.4. P recovery Experiments

Jar test experiments were used to quantify P efficiency from LPWs via CaP crystallization with different seed dosages and at different pH and reaction time. All experiments were carried out in triplicate. A 200 mL aliquot of 1.5 mM CaCl_2 solution was added to an equal volume of LPWs in Perspex vessel (500 mL), resulting in initial Ca^{2+} and P concentrations of 30 mg/L and 1 mg/L, respectively. Determined amounts of HAP (0–10 g/L for seed dosages tests and 5 g/L for reaction time tests, respectively) were introduced into mixtures. pH value was adjusted to target value, and ionic strength $I = 0.02$ M. Temperature was controlled at 298 ± 0.5 K. CaP crystallization was immediately triggered by mechanical stirring at 200 rpm. For seed dosages tests, reaction lasted for 30 min, and 5 mL aliquots were withdrawn for measuring P concentration. For reaction time tests, CaP crystallization was quenched at 1, 5, 10, 30, 60, and 90 min, respectively, and 5 mL aliquots were withdrawn immediately.

2.5. Characterization and Analysis

P concentration was determined using the molybdenum blue spectrophotometric method with a UV–Vis spectrophotometer (SPECTRA UV-11, MRC, Youke, Shanghai, China) at 700 nm. P recovery efficiency was calculated according to the difference between initial and residual P concentration. Scanning electron microscopy (SEM), energy dispersive spectrometry (EDS), and X-ray diffraction (XRD) analyses were conducted for original seed particles and P recovery products at seed dosage of 2 g/L and reaction time of 30 min, to determine their physicochemical properties. For P recovery products, after P recovery was completed 10 mL reaction mixture was withdrawn and filtered through a 0.22 μm filter. The sample was then rinsed with a few drops of deionized water to remove the remaining $\text{Na}_2\text{HPO}_4/\text{CaCl}_2$ solution, and then rapidly dried and stored in a desiccator. For original seed particles, no pretreatment was demanded. The surface morphologies of specimens were determined with SEM-EDS using a S-4800 scanning electron microscope (Hitachi, Tokyo, Japan), with an accelerating voltage of 15.0 kV. The chemical morphologies of specimens were characterized with a Smartlab-9 kw powder diffractometer (Rigaku, Tokyo, Japan). The angles were scanned from 5° to 90° at a speed of 2° min^{-1} .

3. Results and Discussion

3.1. Kinetics of P Adsorption in LPWs

The dynamics of P concentration for experiments with various initial P concentration and HAP dosage are shown in Figure 1. Figure 1a indicates that it was definitely HAP dissolution, not P adsorption that occurred when initial P concentration was no higher than 5 mg/L. For the initial P concentration of 25 mg/L, no significant changes in P concentration were detected, suggesting an equilibrium between HAP dissolution and P adsorption/crystallization, in this case. HAP dissolution was further confirmed, as shown in Figure 1b, considering the high initial HAP dosage and the higher equilibrium with P concentration. The fitting results of the kinetic models are depicted in Tables S1–S3. The pseudo-second-order kinetic model fitted best with the experimental dates, except for the initial P concentration of 25 mg/L. The calculated q_e values agreed very well with the experimental ones. The invalid description for the initial P concentration of 25 mg/L clearly suggested other simultaneous processes, which may be P adsorption or CaP crystallization.

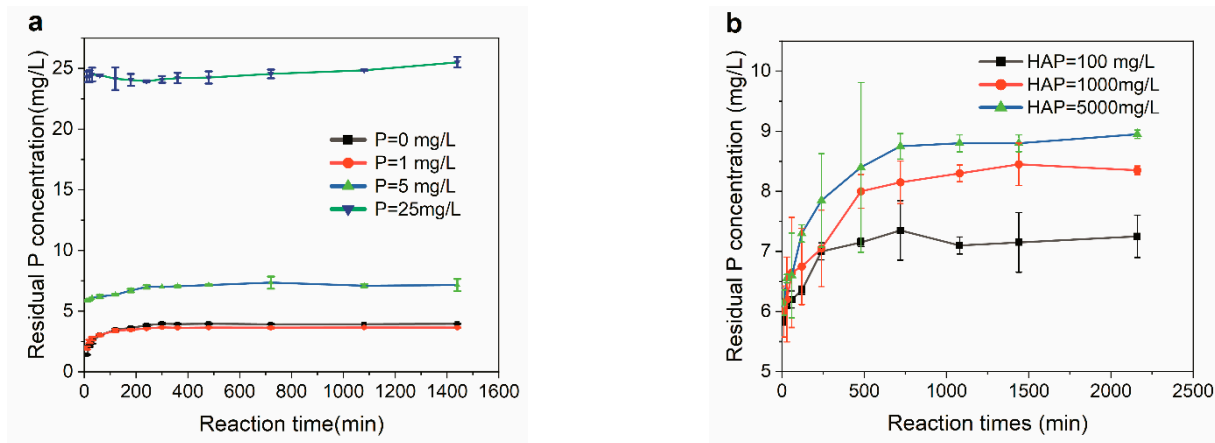


Figure 1. Phosphorus adsorption/dissolution kinetics under different initial P concentrations with HAP dosage of 100 mg/L (a) and different HAP dosage with initial P concentrations of 5 mg/L (b).

The obtained values for Langmuir and Freundlich isotherm constants and correlation coefficients were listed in Table S4. The results showed that the correlation coefficient (R^2) of the Freundlich isotherm was higher than that of the Langmuir isotherm, demonstrating that HAP dissolution could be described better using the former. The negative value for ΔH^0 (-3.93 kJ/mol) indicated HAP dissolution was an exothermic process (Table S5). The negative values of ΔS^0 (-11.3 J/(mol K)) indicated a regular increase in the randomness during HAP dissolution, which can be interrupted by the hydration process of dissolved ions. To our knowledge, this paper is the first report on the dissolution of apatite in P-containing wastewater. For P recovery from LPWs using apatite as the seed, the adsorption mechanism can be ruled out.

3.2. Role of Ca^{2+} Introduction

For constant pH titration experiments at each initial Ca^{2+} concentration, significant OH^- consumption was detected within the first 60 s (Figure 2a), suggesting an obvious and rapid deprotonation process, i.e., CaP crystallization occurred in LPWs. Rapid CaP crystallization was further confirmed by the results shown in Figure 2b, as over 70% of the P was recovered within 60 s. The excellent P recovery also confirmed that no HAP dissolution occurred in LPWs, indicating the prominent suppressing effect of Ca^{2+} on HAP dissolution.

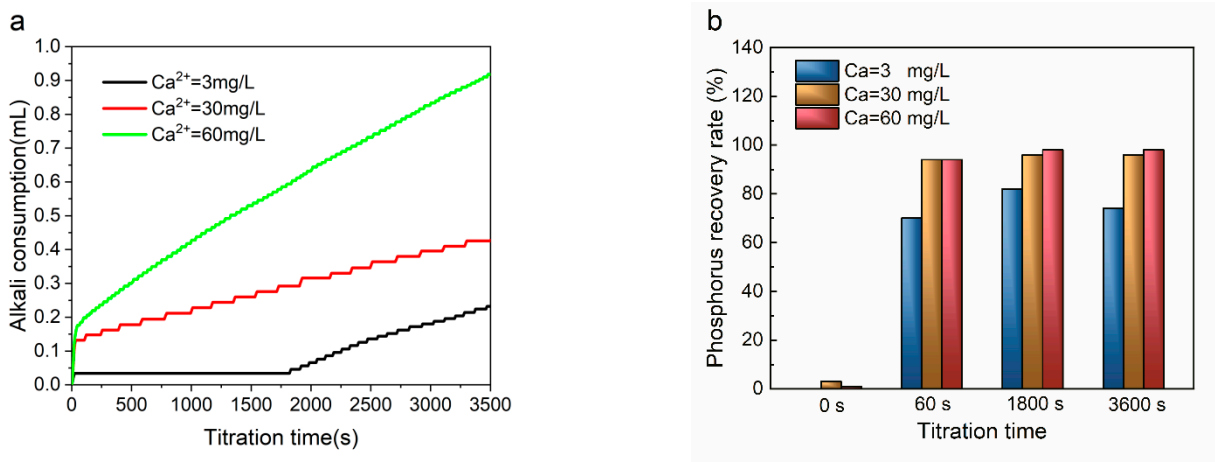


Figure 2. Effects of initial Ca^{2+} concentrations on alkali consumptions (a) and phosphorus recovery efficiencies (b) for constant pH titration experiments with initial P concentration of 1 mg/L, HAP dosage of 2 g/L, and constant pH of 9.0.

To our surprise, up to 70% P was recovered within the first 60 s at 3 mg/L Ca^{2+} , while the corresponding OH^- consumption was only 0.04 mL. The calculated crystallization rates based on OH^- consumptions showed the minimum crystallization rate at 3 mg/L Ca^{2+} (Figure S1), not matching its good P recovery effect. Apatite was reported to include acidic and alkaline forms. The latter form is HAP and the former are several precursor phases of HAP [36]. A more acidic apatite phase was detected at lower Ca/P molar ratio [36], indicating smaller OH^- consumption during its formation. Therefore, we postulated different apatite phases occurred presently. The most acidic phase might form at 3 mg/L Ca^{2+} , exhibiting the smallest OH^- consumption. It is also worth pointing out that continuous OH^- consumptions were observed after the first sharp consumption. Carino et al. [37] reported the same phenomenon in their research on the formation and transformation of CaP phases. They attributed the continuous OH^- consumption to phase transformation from acidic apatite to HAP. During apatite phases transformation, P concentration of bulk liquid should be almost constant, as such a process is realized via reorganization of lattice ions and/or apatite clusters [38], which explains the constant P recovery efficiency after the first 60 s (Figure 2b).

While for the non-constant pH titration experiment, an obvious decrease in pH and electrical conductivity was observed during the first 80 s and 20 s, respectively (Figures S2 and S3). The simultaneous decrease in a short time undoubtedly denoted the CaP crystallization. Interestingly, the change in pH seemed to lag behind that in electrical conductivity, which may be caused by the good buffer capacity of $\text{HPO}_4^{2-}/\text{PO}_4^{3-}$.

3.3. Effect of Seed Dosage, Crystallization Time, and pH on P Recovery

P recovery efficiencies at various seed dosages, precipitation time and pH are shown in Figure 3a,b. Compared to the absence of seed, pronounced P recovery was achieved at sufficient seeds dosage (Figure 3a), in line with previous studies [22,24,39]. No significant difference was observed between dosage of 5 g/L and 10 g/L ($p > 0.05$), suggesting 5 g/L being sufficient. For high P-containing wastewaters, larger seed dosage provides more active crystalline sites facilitating surface-induced crystallization (SIC) and thus higher P recovery efficiency [40]. For LPWs, the more active crystalline sites may result in their competition for limited P, decreasing P concentration within seeds' hydration shells, wherein CaP crystallizes, consequently suppressing CaP crystallization [41]. Considering the continuous increasing P recovery efficiency (Figure 3a), it is reasonable to conclude that SIC is not the main underlying mechanism for CaP crystallization. In fact, SIC is usually considered as the subsequent process of surface P adsorption during P recovery [1,42]. It was the dissolution of HAP, not the adsorption of P, that came into prominence for LPWs, further confirming the negligible role of SIC. On the contrary, the continuous increase in P recovery efficiency with seed dosages seemed to follow PNCs aggregation mechanism well, where P recovery is achieved via the aggregation between PNCs and seeds. Higher seed dosage improves the aggregation scale, leading to higher P recovery efficiency. Similar operations have been reported by Dai et al. [41], wherein the aggregation improvement was achieved by air agitation.

A P recovery efficiency of over 70% was achieved within the first 1 min (Figure 3b), suggesting rapid P recovery once the seeds were introduced. By further prolonging reaction time to 30 min, P recovery efficiency increased to 85%; after that, no significant improvement was observed ($p > 0.05$). The rapid P recovery confirmed again that SIC played a negligible role in P recovery. It is not hard to imagine that the rates of both P adsorption and CaP crystallization on seed particle surfaces, if existing, were severely reduced by the low initial P concentration of LPWs. However, the aggregation between PNCs and seed particles can be anticipated to be accomplished within 1 min, providing there are sufficient seed dosages and mechanical stirring strength.

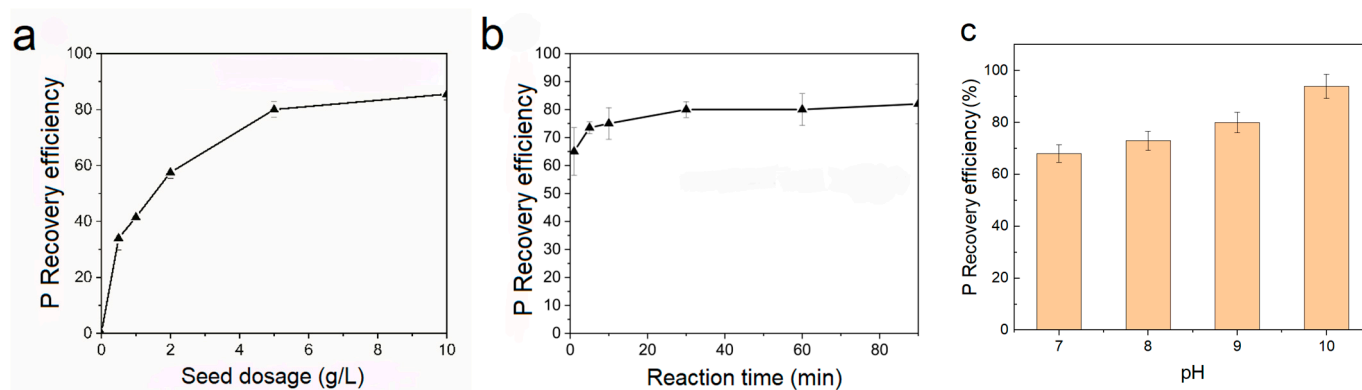


Figure 3. Effects of HAP dosages (a), reaction time (b) and pH (c) on phosphorus recovery efficiencies from LPWs via CaP crystallization. For HAP dosage tests, reaction time was 30 min; for reaction time tests, HAP dosage was 5 g/L. Initial Ca^{2+} and P concentrations were 30 mg/L and 1 mg/L, respectively, and initial pH was 9.0 in each test.

Within a pH of 7–9, P recovery efficiency increased with the enhancement of pH, though not significantly ($p > 0.05$), indicating the key role of CaP crystallization in P recovery once again since high pH facilitates CaP crystallization.

3.4. Characteristics of Seed Particles and P Recovery Products

The morphologies of P recovery products at a seed dosage of 2 g/L and a reaction time of 30 min, together with the original seeds, were examined by SEM. Figure S4a,b illustrate that the original seeds are particles with a regular spherical shape and rough surfaces, of which the particle size ranges from tens of micrometers to about one hundred micrometers. The rough surface is composed of a layer of rod-shaped fines with sizes of approximately dozens of nanometers (Figure S4b). Almost no changes in seed size distribution were observed after P recovery (Figure S4c), which could be well interpreted by the fact that the initial P concentration was only 1 mg/L. In addition, the rod-shaped fines on the seed surface became denser and smaller compared to those of the original seeds (Figure S4d). It was postulated that the formation of such smaller fines was the result of CaP crystallization rather than the dissolution of fines shown in Figure S4b, considering the aforementioned suppressive effects of Ca^{2+} on HAP dissolution. Such postulation could be further supported by the EDS (Figure S4e,f) and XRD (Figure S4g) spectrum of original seed and P recovery products. The EDS spectrum indicated C, O, P, and Ca as the main constituent elements of both samples, while the XRD spectrum of both samples exhibited typical peaks of HAP and its precursors such as ACP and OCP at 24.92° , 26.99° , and 32.78° .

The accumulation of a large amount of dense and small fines on the seed surface prompted us to associate P removal with the aggregation of CaP PNCs, the so-called Posner's clusters with sizes between 0.7 and 1.0 nm in the solution [43]. Several documents have reported the aggregation of CaP PNCs [43–45]. However, the particle size of fines shown in Figure S4d is about two orders of magnitude larger than that of CaP PNCs, indicating they should not be PNCs themselves. We hypothesized the fines might be the preliminary or secondary aggregating products of CaP PNCs, before which CaP PNCs accumulated on the seed surfaces via aggregation with seeds.

At present, the XRD spectra of seeds before and after P recovery both exhibited typical peaks of calcite (Figure S4g). In addition, C molar content was elevated from 0.68% to 7.24% after P recovery (Figure S4e,f), indicating the simultaneous crystallization of calcite with CaP. Carbonate has been reported to be one of the main coexisting impurities in P-containing wastewater [46]. During P recovery, carbonate competes with P for free Ca^{2+} , inhibiting CaP nucleation and consequently reducing P recovery efficiency [47]. Atmospheric CO_2 can be captured directly by basic solution [48], interpreting the present calcite crystallization, despite the carbonate absence in the original LPWs. Nonetheless, it

is necessary to stem the co-crystallization of calcite, which may severely reduce the purity and quality of P recovery products.

3.5. P Recovery Mechanism from LPWs via CaP Using Apatite

According to the obtained results, the underlying mechanism for P recovery from LPWs via CaP crystallization using apatite as the seed is shown in Figure 4. Upon the introduction of adequate Ca^{2+} into LPWs containing apatite, P begins to aggregate with Ca^{2+} quickly, generating CaP PNCs, while the surplus excessive Ca^{2+} exhibit their continuous inhibitory effects on apatite dissolution. P recovery from LPWs starts with the aggregation between CaP PNCs and seed particles, leading to CaP PNCs densification on the seed surfaces. In a next step, the further densification of CaP PNCs results in their fusion, i.e., the formation of preliminary aggregating products. At this moment, the irregular solid–liquid interface occurs. Ultimately, preliminary aggregating products transform into fines via secondary aggregating, exhibiting rod-shaped morphology with sizes of approximately dozens of nanometers (Figure S4d).

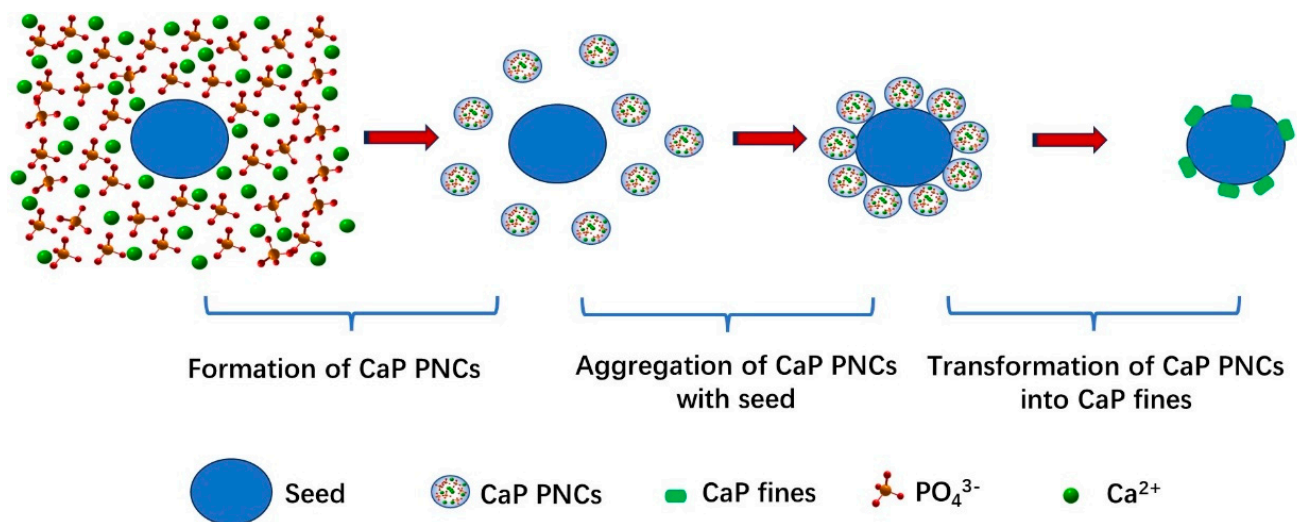


Figure 4. Possible mechanism for P recovery from LPWs via CaP crystallization using apatite as seed.

A comparable description of CaP crystallization via PNCs aggregation has been documented by Dey et al. [49], where the densification of PNCs takes place on the surface of the organic template and the driving force of the densification is reported to be the attractiveness of the organic templates to PNCs. At present, the PNCs densification occurred at the seed surface and was suggested to be driven mainly by aggregation between PNCs and seed particles. Because of the continuous mechanical stirring in LPWs, PNCs and seed particles collide with each other with high frequency, leading to significant aggregation between them.

In addition to this, the attractiveness of active Ca and P sites at the seed surface may also play a partial role for the densification of PNCs. Indeed, HAP is commonly used as a seed material for P recovery from wastewater via CaP crystallization [19,20,24]. In this case, HAP particles possess similar lattice structure as CaP crystalline products, therefore they exhibit higher molecular recognition ability and consequently, more excellent attractiveness to crystalline products, compared to other seed materials such as calcite and sand.

The formation of PNCs has been widely reported in unsaturated solutions such as LPWs [45,50]. In addition, PNCs aggregation mechanism reasonably explains our experimental results. Unfortunately, we did not directly observe PNCs and their aggregation processes. Further research based on cryo TEM observation should be conducted to accurately reveal the P recovery mechanism from LPWs via CaP crystallization using apatite as the seed.

4. Conclusions

This study demonstrated that, when using HAP as seed, PNCs aggregation with seed particles is responsible for P recovery from LPWs via CaP crystallization. HAP adsorption/dissolution kinetic experiments, titration experiments, and P recovery experiments demonstrated the following key findings:

- It was HAP dissolution, rather than P adsorption, that occurred when the initial P concentration of LPWs was no higher than 25 mg/L, ruling out the adsorption mechanism for P recovery from LPWs via CaP crystallization using HAP as the seed.
- The dissolution of HAP in LWP with an initial P concentration no higher than 25 mg/L, an exothermic and entropy reduction driven process, followed the pseudo-second-order kinetic model well. Introducing Ca^{2+} suppressed the dissolution of HAP effectively, and CaP crystallization occurred.
- It is PNCs' aggregation, not surface-induced crystallization, that plays the key role in P recovery from LPWs via CaP crystallization using HAP as the seed.
- During PNCs aggregation, P aggregates with Ca^{2+} quickly, generating CaP PNCs; then, CaP PNCs aggregate with seed particles, followed by CaP PNCs fusion, and they ultimately transform into rod-shaped fines attached to the seed surface.

Supplementary Materials: The following supporting information can be downloaded at: <https://www.mdpi.com/article/10.3390/separations11050138/s1>, Figure S1: Effect of initial Ca concentration on alkali consumption rates during constant pH titration experiments; Figure S2: The change of pH during non-constant pH titration experiment; Figure S3: The change of electrical conductivity during non-constant pH titration experiment; Figure S4: Characteristics of original seeds and P recovery products. (a) and (b) are SEM images of original seeds with magnification of $\times 200$ and $\times 50,000$, respectively. (c) and (d) are SEM images of P recovery products with magnification of $\times 200$ and $\times 50,000$, respectively. (e) and (f) are EDS spectra for C, O, P, K and Ca of original seeds and P recovery products, respectively. (g) is X-ray diffraction diagrams of original seeds and P recovery products. P recovery test conditions: initial P concentration of 1 mg/L, initial Ca^{2+} concentration of 30 mg/L, initial pH of 9.0, seed dosage of 2 g/L, and reaction time 30 min; Table S1: Dissolution kinetic parameters of pseudo-first-order dynamics model; Table S2: Dissolution kinetic parameters of pseudo-second-order dynamics model; Table S3: Dissolution kinetic parameters of intra-particle diffusion model; Table S4: Parameters of dissolution isotherms at different temperatures; Table S5: Thermodynamic parameters of HAP dissolution at different temperatures.

Author Contributions: X.N., conceptualization, data curation, formal analysis, funding acquisition, methodology, writing—original draft, writing—review and editing; Y.L., data curation, formal analysis, funding acquisition, validation, writing—original draft; J.W., data curation, methodology; S.O., formal analysis, validation; Z.W., formal analysis, validation; G.W., formal analysis, validation; H.J., formal analysis, validation. All authors have read and agreed to the published version of the manuscript.

Funding: This work is supported by the Environmental Protection Research Project of Hunan Province (HBKT-2022001), Major Science and Technology Projects of the Ministry of Water Resources of China (SKS-2022079), Special fund for building Chenzhou National Sustainable Development Agenda Innovation Demonstration Zone in Hunan Province (2022sfq51), and Double First Class Construction Project of Changsha university of science and technology (Project Contract NO. 2022040212).

Data Availability Statement: The original contributions presented in the study are included in the article/supplementary material, further inquiries can be directed to the corresponding author/s.

Conflicts of Interest: Author Heng Jiang was employed by the company Hunan Water Resources and Hydropower Survey, Design, Planning and Research Co., Ltd., The remaining authors declare that the research was conducted in the absence of any commercial or financial relationships that could be construed as a potential conflict of interest.

References

1. Pap, S.; Zhang, H.Y.; Bogdan, A.; Elsby, D.T.; Gibb, S.W.; Bremner, B.; Taggart, M.A. Pilot-scale phosphate recovery from wastewater to create a fertiliser product: An integrated assessment of adsorbent performance and quality. *Water Res.* **2022**, *228*, 119369. [[CrossRef](#)] [[PubMed](#)]
2. Cui, J.L.; Yang, J.S.; Weber, M.; Yan, J.; Li, R.H.; Chan, T.S.; Jiang, Y.; Xiao, T.F.; Li, X.Y.; Li, X.D. Phosphate interactions with iron-titanium oxide composites: Implications for phosphorus removal/recovery from wastewater. *Water Res.* **2023**, *234*, 119804. [[CrossRef](#)] [[PubMed](#)]
3. U.S. Geological Survey. *Mineral Commodity Summaries 2021*; U.S. Geological Survey: Reston, VA, USA, 2021.
4. Capua, F.D.; Sario, S.D.; Ferraro, A.; Petrella, A.; Race, M.; Pirozzi, F.; Fratino, U.; Spasiano, D. Phosphorous removal and recovery from urban wastewater: Current practices and new directions. *Sci. Total. Environ.* **2022**, *823*, 153750. [[CrossRef](#)] [[PubMed](#)]
5. Tang, Q.; Yin, Z.; Wang, R.D.; Zhu, W.; Zhang, Z.P.; Wang, Y.; Yang, Z.; Liu, F.Q.; Yang, W.B. New Strategy to Remove Phosphate from Low Concentration Solution by MOFs-Modified Resin: High Affinity and Thermal Desorption. *Chem. Eng. J.* **2023**, *465*, 142864. [[CrossRef](#)]
6. Singh, A.K.; Kumar, A.; Bilal, M.; Chandra, R. Organometallic pollutants of paper mill wastewater and their toxicity assessment on Stinging catfish and sludge worm. *Environ. Technol. Inno.* **2021**, *24*, 101831. [[CrossRef](#)]
7. Xu, M.; Gao, P.; Chen, H.Q.; Huang, X.H.; Xue, Z.X.; Shen, X.X.; Li, C.; Cao, J.S. Spatiotemporal distribution of microorganisms in a full-scale anaerobic baffled reactor–anoxic/oxic treatment plant for printing and dyeing wastewater. *J. Water. Process. Eng.* **2022**, *49*, 103090. [[CrossRef](#)]
8. Zou, R.; Tang, K.; Hambly, A.C.; Wunsch, U.J.; Andersen, H.R.; Angelidaki, I.; Zhang, Y.F. When microbial electrochemistry meets UV: The applicability to high-strength real pharmaceutical industry wastewater. *J. Hazard. Mater.* **2022**, *423*, 127151. [[CrossRef](#)] [[PubMed](#)]
9. Hermassi, M.; Valderrama, C.; Dosta, J.; Cortina, J.L.; Batis, N.H. Evaluation of hydroxyapatite crystallization in a batch reactor for the valorization of alkaline phosphate concentrates from wastewater treatment plants using calcium chloride. *Chem. Eng. J.* **2015**, *267*, 142–152. [[CrossRef](#)]
10. Xie, M.; Shon, H.K.; Gray, S.R.; Elimelech, M. Membrane-based processes for wastewater nutrient recovery: Technology, challenges, and future direction. *Water Res.* **2016**, *89*, 210–221. [[CrossRef](#)]
11. Huang, W.; Zhang, Y.; Li, D. Adsorptive removal of phosphate from water using mesoporous materials: A review. *J. Environ. Manage.* **2017**, *193*, 470–482. [[CrossRef](#)]
12. Rotta, E.H.; Bitencourt, C.S.; Marder, L.; Bernardes, A.M. Phosphorus recovery from low phosphate-containing solution by electrodialysis. *J. Membrane. Sci.* **2019**, *573*, 293–300. [[CrossRef](#)]
13. Cheng, P.; Liu, Y.; Yang, L.; Wang, X.; Chi, Y.B.; Yuan, H.L.; Wang, S.B.; Ren, Y.X. Adsorption and recovery of phosphate from aqueous solution by katoite: Performance and mechanism. *Colloid. Surface. A* **2022**, *655*, 130285. [[CrossRef](#)]
14. Pronk, W.; Biebow, M.; Boller, M. Electrodialysis for Recovering salts from a urine solution containing micropollutants. *Environ. Sci. Technol.* **2006**, *40*, 2414–2420. [[CrossRef](#)] [[PubMed](#)]
15. Wang, X.L.; Wang, Y.M.; Zhang, X.; Feng, H.Y.; Li, C.R.; Xu, T.W. Phosphate recovery from excess sludge by Conventional Electrodialysis (CED) and electrodialysis with Bipolar Membranes (EDBM). *Ind. Eng. Chem. Res.* **2013**, *52*, 15896–15904. [[CrossRef](#)]
16. Zhang, Y.; Desmidt, E.; Loooveren, A.V.; Pinoy, L.; Meesschaert, B.; Bruggen, B.V.D. Phosphate separation and recovery from wastewater by novel electrodialysis. *Environ. Sci. Technol.* **2013**, *47*, 5888–5895. [[CrossRef](#)] [[PubMed](#)]
17. Bellier, N.; Chazarenc, F.; Comeau, Y. Phosphorus removal from wastewater by mineral apatite. *Water Res.* **2006**, *40*, 2965–2971. [[CrossRef](#)] [[PubMed](#)]
18. Guo, Y.; Li, Y.Y. Hydroxyapatite crystallization-based phosphorus recovery coupling with the nitrogen removal through partial nitrification/anammox in a single reactor. *Water Res.* **2020**, *187*, 116444. [[CrossRef](#)]
19. Xiao, H.Y.; Nie, X.B.; Wan, J.L.; Deng, Q.Q.; Wang, Y.R.; Long, Y.N.; Jiang, C.B. Phosphorous recovery from wastewater with low phosphorous concentration by means of HAP-seeded crystallization of calcium phosphate. *China Environ. Sci.* **2022**, *42*, 1681–1687. (In Chinese)
20. Song, Y.H.; Donnert, D.; Berg, U.; Weidler, P.G.; Nueesch, R. Seed selections for crystallization of calcium phosphate for phosphorus recovery. *J. Environ. Sci.* **2007**, *19*, 591–595. [[CrossRef](#)]
21. Karapinar, N.; Hoffmann, E.; Hahn, H.H. Magnetite seeded precipitation of phosphate. *Water Res.* **2004**, *38*, 3059–3066. [[CrossRef](#)]
22. Kim, E.H.; Lee, D.W.; Hwang, H.K.; Yim, S. Recovery of phosphates from wastewater using converter slag: Kinetics analysis of a completely mixed phosphorus crystallization process. *Chemosphere* **2006**, *63*, 192–201.
23. Dai, H.L.; Lv, X.W.; Gao, Q.N. Phosphorus recovery from anaerobic supernatant of EBPR process based on HAP crystallization. *J. Southeast Univ.* **2016**, *46*, 1020–1026. (In Chinese)
24. Jang, H.; Kang, S.H. Phosphorus removal using cow bone in hydroxyapatite crystallization. *Water Res.* **2002**, *36*, 1324–1330.
25. Molle, P.; Liénard, A.; Grasmick, A.; Iwema, A.; Kabbabi, A. Apatite as an interesting seed to remove phosphorus from wastewater in constructed wetlands. *Water Sci. Technol.* **2005**, *51*, 193–203. [[CrossRef](#)]
26. Boeykens, S.P.; Piol, M.N.; Legal, L.S.; Saralegui, A.B.; Vázquez, C. Eutrophication decrease: Phosphate adsorption processes in presence of nitrates. *J. Environ. Manage.* **2017**, *203*, 888–895.
27. Park, J.H.; Wang, J.J.; Xiao, R.; Zhou, B.Y.; Delaune, R.D.; Seo, D.C. Effect of pyrolysis temperature on phosphate adsorption characteristics and mechanisms of crawfish char. *J. Colloid. Interf. Sci.* **2018**, *525*, 143–151.

28. Søvik, A.K.; Kløve, B. Phosphorus retention processes in shell sand filter systems treating municipal wastewater. *Ecol. Eng.* **2005**, *25*, 168–182. [[CrossRef](#)]
29. Lu, S.G.; Bai, S.Q.; Zhu, L.; Shan, H.D. Removal mechanism of phosphate from aqueous solution by fly ash. *J. Hazard. Mater.* **2009**, *161*, 95–101.
30. Leng, L.J.; Zhang, J.Q.; Xu, S.Y.; Xiong, Q.; Xu, X.W.; Li, J.N.; Huang, H.J. Meat & bone meal (MBM) incineration ash for phosphate removal from wastewater and afterward phosphorus recovery. *J. Clean. Prod.* **2019**, *238*, 117960.
31. Yang, M.G.; Shi, J.; Xu, Z.W.; Zhu, S.Y.; Cui, Y.X. Phosphorus removal and recovery from fosfomycin pharmaceutical wastewater by the induced crystallization process. *J. Environ. Manage.* **2019**, *231*, 207–212. [[CrossRef](#)]
32. Deng, Q.Q.; Nie, X.B.; Wan, J.L.; Xiao, H.Y.; Xiao, D.F.; Liao, M.F.; Liu, W.Q. Influence of induced-crystallization reactor styles on phosphorous recovery from wastewater with low phosphorous concentration. *China Environ. Sci.* **2023**, *43*, 2296–2302. (In Chinese)
33. Gao, Z.G.; Wu, Y.; Wu, Y.Y.; Gong, J.B.; Bao, Y.; Wang, J.K.; Rohani, S. Self-induced nucleation during the antisolvent crystallization process of candesartan cilexetil. *Cryst. Growth. Des.* **2018**, *18*, 7655–7662. [[CrossRef](#)]
34. Gebauer, D.; Kellermeier, M.; Cölfena, H.; Gale, J.D.; Bergström, L. Pre-nucleation clusters as solute precursors in crystallisation. *Chem. Soc. Rev.* **2014**, *43*, 2348–2371. [[CrossRef](#)]
35. Kellermeier, M.; Gebauer, D.; Melero-García, E.; Drechsler, M.; Talmon, Y.; Kienle, L.; Cölfen, H.; García-Ruiz, J.M.; Kunz, W. Colloidal stabilization of calcium carbonate prenucleation clusters with Silica. *Adv. Funct. Mater.* **2012**, *22*, 4301–4311. [[CrossRef](#)]
36. Ge, X.F.; Wang, L.J.; Zhang, W.J.; Putnis, C.V. Molecular Understanding of Humic Acid-Limited Phosphate Precipitation and Transformation. *Environ. Sci. Technol.* **2020**, *54*, 207–215. [[CrossRef](#)]
37. Carino, A.; Ludwig, C.; Cervellino, A.; Müller, E.; Testino, A. Formation and transformation of calcium phosphate phases under biologically relevant conditions: Experiments and modeling. *Acta. Biomater.* **2018**, *74*, 478–488. [[CrossRef](#)]
38. Ito, N.; Kamitakahara, M.; Yoshimura, M.; Ioku, K. Importance of nucleation in transformation of octacalcium phosphate to hydroxyapatite. *Mat. Sci. Eng. C Mater.* **2014**, *40*, 121–126. [[CrossRef](#)]
39. Song, Y.H.; Hahn, H.H.; Hoffmann, E. The effect of carbonate on the precipitation of calcium phosphate. *Environ. Technol.* **2002**, *23*, 207–215. [[CrossRef](#)]
40. Song, Y.H.; Hahn, H.H.; Hoffmann, E. Effects of solution conditions on the precipitation of phosphate for recovery A thermodynamic evaluation. *Chemosphere* **2002**, *48*, 1029–1034. [[CrossRef](#)] [[PubMed](#)]
41. Dai, H.L.; Lv, X.W.; Peng, Y.H.; Zou, H.M.; Shi, J. An efficient approach for phosphorus recovery from wastewater using series-coupled air-agitated crystallization reactors. *Chemosphere* **2016**, *165*, 211–220. [[CrossRef](#)]
42. Pap, S.; Gaffney, P.P.J.; Bremner, B.; Sekulic, M.T.; Maletic, S.; Gibb, S.W.; Taggart, M.A. Enhanced phosphate removal and potential recovery from wastewater by thermo-chemically calcinated shell adsorbents. *Sci. Total. Environ.* **2022**, *814*, 152794. [[CrossRef](#)] [[PubMed](#)]
43. Zhang, H.L.; Zhao, C.S.; Wang, Y.P.; Sheng, G.P. Observing the Biologically Induced Phosphate Precipitation by Sludge Extracellular Polymeric Substances in Enhanced Biological Phosphorus Removal. *ACS. EST. Eng.* **2022**, *2*, 1514–1522. [[CrossRef](#)]
44. Wang, L.J.; Li, S.; Ruiz-Agudo, E.; Putnis, C.V.; Putnis, A. Posner’s cluster revisited: Direct imaging of nucleation and growth of nanoscale calcium phosphate clusters at the calcite-water interface. *Cryst. Eng. Comm.* **2012**, *14*, 6252–6256. [[CrossRef](#)]
45. Garcia, N.A.; Malini, R.I.; Freeman, C.L.; Demichelis, R.; Raiteri, P.; Sommerdijk, N.A.J.M.; Harding, J.H.; Gale, J.D. Simulation of calcium phosphate prenucleation clusters in aqueous solution: Association beyond ion pairing. *Cryst. Growth. Des.* **2019**, *19*, 6422–6430. [[CrossRef](#)] [[PubMed](#)]
46. Vasenko, L.; Qu, H.Y. Enhancing the recovery of calcium phosphates from wastewater treatment systems through hybrid process of oxidation and crystallization. *J. Environ. Chem. Eng.* **2019**, *7*, 102828. [[CrossRef](#)]
47. Cao, X.; Harris, W. Carbonate and magnesium interactive effect on calcium phosphate precipitation. *Environ. Sci. Technol.* **2008**, *42*, 436–442. [[CrossRef](#)] [[PubMed](#)]
48. Burhenne, L.; Giacomini, C.; Follett, T.; Ritchie, J.; McCahill, J.S.J.; Mérida, W. Characterization of reactive CaCO₃ crystallization in a fluidized bed reactor as a central process of direct air capture. *J. Environ. Chem. Eng.* **2017**, *5*, 5968–5977. [[CrossRef](#)]
49. Dey, A.; Bomans, P.H.H.; Muller, F.A.; Will., J.; Frederik, P.M.; With, G.D.; Sommerdijk, N.A.J.M. The role of prenucleation clusters in surface-induced calcium phosphate crystallization. *Nat. Mater.* **2010**, *9*, 1010–1014. [[CrossRef](#)]
50. Yang, X.; Wang, M.Z.; Yang, Y.; Cui, B.L.; Xu, Z.J.; Yang, X.N. Physical origin underlying the prenucleation-cluster-mediated nonclassical nucleation pathways for calcium phosphate. *Phys. Chem. Chem. Phys.* **2019**, *21*, 14530–14540. [[CrossRef](#)]

Disclaimer/Publisher’s Note: The statements, opinions and data contained in all publications are solely those of the individual author(s) and contributor(s) and not of MDPI and/or the editor(s). MDPI and/or the editor(s) disclaim responsibility for any injury to people or property resulting from any ideas, methods, instructions or products referred to in the content.